Icarus 260 (2015) 1–6

Contents lists available at ScienceDirect

Icarus

journal homepage: www.elsevier.com/locate/icarus

Goldstone radar imaging of near-Earth Asteroid 2003 MS2

Kenneth J. Lawrence *, Lance A.M. Benner, Marina Brozovic, Steven J. Ostro, Joseph S. Jao, Jon D. Giorgini, Martin A. Slade, Raymond F. Jurgens

Jet Propulsion Laboratory, California Institute of Technology, Pasadena, CA 91109-8099, USA

ARTICLE INFO

Article history:
Received 3 March 2015
Revised 30 May 2015
Accepted 2 June 2015
Available online 12 June 2015

Keywords:
Radar observations
Asteroids, rotation
Asteroids, surfaces

ABSTRACT

We report radar observations of near-Earth Asteroid (NEA) 2003 MS2 with Goldstone (8560 MHz, 3.5 cm) on June 28, 29, and July 4, 2003, shortly after the asteroid's discovery. Delay-Doppler images with resolutions as fine as 19 m/pixel reveal an unusually angular object with pronounced facets. The longest sequence of images was obtained on July 4 when the asteroid rotated ~140 deg in 2.7 h. During this interval, bandwidths varied by a factor of ~1.5 and indicate that 2003 MS2 is an elongated object. The rotation and bandwidth variations evident in the radar images are consistent with the 7 h rotation period and the 0.7 magnitude lightcurve amplitude reported by Muinonen et al. (Muinonen, K. et al. [2007]. Spins, shapes, and orbits for near-Earth objects by Nordic NEON. In: Milani, A., Valsecchi, G.B., Vokrouhlický, D. (Eds.), Near Earth Objects, our Celestial Neighbors: Opportunity and Risk. Cambridge University Press, Cambridge, pp. 309–320). If we adopt the 7 h period, then the maximum and minimum bandwidths place lower bounds on the pole-on dimensions of (0.33×0.19) km/cos δ, where δ is the unknown subradar latitude. The radar and photometric observations by Muinonen et al. constrain the pole directions to $(\lambda, \beta) = (20 \pm 20$ deg, 0 ± 40 deg) and $(200 \pm 20$ deg, 0 ± 40 deg). The circular polarization ratio of 0.31 ± 0.02 is comparable to that of 25143 Itokawa, suggesting a similar degree of near-surface roughness at decimeter spatial scales.

1. Introduction

Near-Earth Asteroid 2003 MS2 was discovered on June 25, 2003 at Lowell Observatory by the LONEOS program one week before the asteroid's close encounter at a distance of 0.025 au on July 2. Archive searches later identified two pre-discovery images from March 7 at Apache Point Observatory. The Minor Planet Center classified 2003 MS2 as a "potentially hazardous asteroid" with a semi-major axis of 1.04 au, an eccentricity of 0.13, an orbital inclination of 20.0 deg, and a perihelion of 0.91 au. Its absolute magnitude of 21.1 (MPEC 2003-M50) suggests a diameter within a factor of two of 0.2 km. Immediately after discovery, we identified 2003 MS2 as a strong radar target at Goldstone with an estimated signal-to-noise ratio (SNR) per day in excess of 500.

Muinonen et al. (2007) reported a rotation period of ~7 h using a 5.9 h lightcurve obtained on January 14, 2005 with the 2.56 m Nordic Optical Telescope at La Palma. They obtained a lightcurve amplitude of 0.7 mag that constrained the aspect ratio (intermediate/long axis) to a maximum of 0.67. To date, the spectral class of 2003 MS2 remains unknown.

2. Observations

The planetary radar system at Goldstone utilizes the 70 m DSS-14 antenna that is part of NASA's Deep Space Network. It is fully steerable and operates in the X band at a frequency of 8560 MHz ($\lambda = 3.5$ cm) (Ostro, 1993). Goldstone is equipped with a transmitter that nominally radiates 440 kW. At the time of the 2003 MS2 discovery announcement, Goldstone was already scheduled to observe near-Earth Asteroid (65909) 1998 FH12. Some of the time when both asteroids were visible was used to observe 2003 MS2 as a target of opportunity. Goldstone observations were obtained on June 28, 29, and July 4 and are summarized in Table 1.

In general, a radar experiment consists of transmit and receive cycles equal in duration to the round-trip-time (RTT) to the object. Each transmit-receive cycle is called a "run" and can be analyzed as a sum of some number of statistically independent measurements of the echo power distribution or "looks." We use two modes of radar observations during the course of our experiment: continuous wave (CW) observations and binary phase coded (BPC) ranging and imaging. During CW observations, we transmit a circularly

* Corresponding author at: Jet Propulsion Laboratory, 4800 Oak Grove Dr., Mail Stop 183-501, Pasadena, CA 91109, USA.
E-mail address: Kenneth.J.Lawrence@jpl.nasa.gov (K.J. Lawrence).

http://dx.doi.org/10.1016/j.icarus.2015.06.001
0019-1035/

Table 1
Radar observations.

Date	Time UTC	Setup	Resolution		RA (deg)	DEC (deg)	Dist. (au)	OSOD	Runs
			μs	Hz					
2003-June-28	10:15:59–10:33:48	CW	–	0.61	181.5	76.3	0.036	7	15
	10:36:39–10:42:01	CW	–	2.4				9	5
	10:54:25–11:04:25	Ranging	10	6.15				9	8
	11:07:48–11:12:18	Ranging	11	5.59				9	4
	11:14:44–11:20:33	Ranging	1	8.20				9	5
2003-June-29	17:55:58–17:59:33	CW	–	0.49	152.0	69.3	0.031	13	4
	18:03:49–18:21:29	Imaging	0.125	1.0				13	16
	18:24:51–18:55:18	Imaging	0.125	0.5				13	29
2003-July-4	18:05:10–18:17:39	CW	–	0.98	118.0	9.3	0.029	17	13
	18:35:06–18:39:45	Ranging	10	6.15				17	5
	18:53:05–18:57:49	Ranging	11	5.59				17	5
	19:04:17–19:20:46	CW	–	0.98				17	17
	19:26:13–19:35:41	CW	–	0.49				19	10
	19:57:54–22:40:02	Imaging	0.125	0.25				19	128

2003 Goldstone radar observations of 2003 MS2. Right ascension (RA), declination (DEC), and geocentric distance are given for each observational setup. OSOD refers to the JPL orbit solution number from the On-Site Orbit Determination software used to update the trajectory estimate. Runs are the number of transmit and receive cycles.

polarized electromagnetic wave of constant amplitude and frequency and receive its reflection from the asteroid in the same sense (SC) and opposite sense (OC) polarizations with respect to the outgoing wave.

The frequency of the reflected wave is dispersed in Doppler frequency due to the asteroid's rotation. The Doppler broadening or bandwidth of the echo is expressed by:

$$B = \frac{4\pi D}{\lambda P}\cos(\delta) \quad (1)$$

where B is the bandwidth of the echo, D is the object's maximum dimension in the plane of sky perpendicular to the radar line of sight, P is the rotational period, λ is the radar wavelength, and δ is the sub-radar latitude.

The BPC mode of observations uses a time-coded waveform that permits the measurement of echo power in both Doppler frequency and time delay. We use BPC waveforms for ranging measurements and for coarse- and high-resolution imaging. The highest resolution delay-Doppler images of 2003 MS2 were obtained with a 0.125 μs time delay setup, corresponding to a range resolution of 18.75 m.

3. Results

The first radar echoes were obtained on June 28, just 3 days after the asteroid's discovery. The initial orbital solution (JPL Horizons solution 7) was determined from 56 optical observations spanning June 25–27, 2003 and provided good pointing constraints (3-σ uncertainty of 1.9 arcsec) for the radar experiment. The initial 3σ Doppler uncertainty was ~4000 Hz, which is large but not unusual for a newly discovered object. The first echo detected indicated a correction to the pre-experiment orbit solution of only −12 Hz (0.009σ). A series of Doppler and ranging corrections to the ephemerides were made throughout the experiment and are summarized in Table 2.

Table 2
Radar astrometry.

Epoch	UTC	Measurement	Sigma	Correction	OSOD
2003-06-28	10:20:00	439594.875	2.0 Hz	−12 Hz	7
2003-06-28	11:00:00	35820178.3	10.0 μs	−162.5 μs	9
2003-06-28	11:20:00	35758682.2	1.0 μs	−161.5 μs	9
2003-06-29	18:00:00	360967.515	1.0 Hz	−1 Hz	13
2003-07-04	18:10:00	−298290.238	2.0 Hz	−10 Hz	17
2003-07-04	18:50:00	29129907.1	10.0 μs	+361.5 μs	17
2003-07-04	22:40:00	29650252.875	1.0 μs	+1.2 μs	19

Radar astrometry for 2003 MS2, which is also posted on the JPL Solar System Dynamics website (http://ssd.jpl.nasa.gov/?radar).

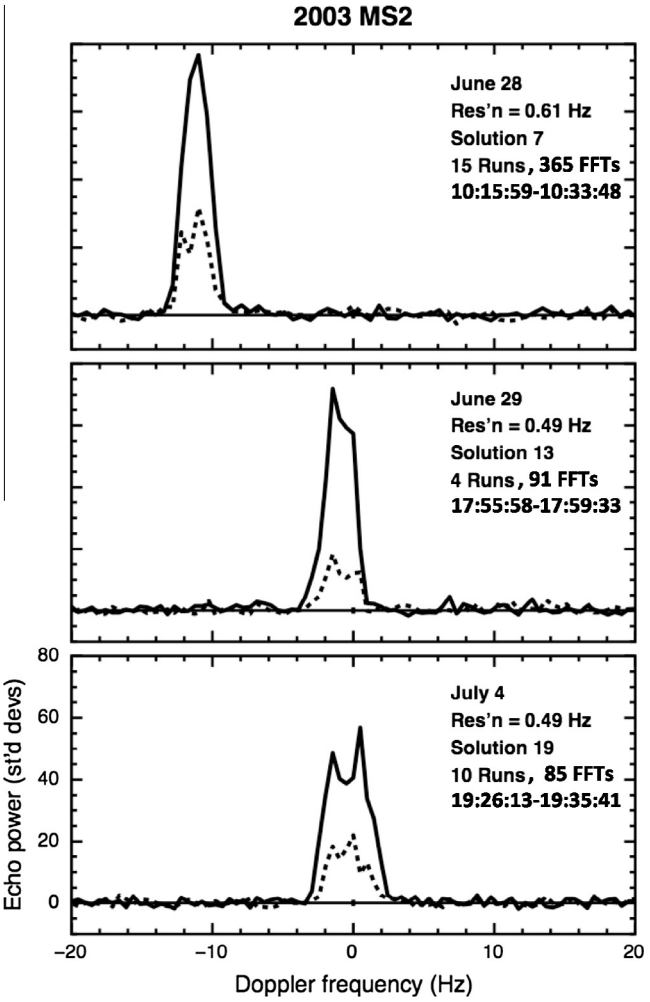

Fig. 1. Goldstone echo power spectra of 2003 MS2. Echo power in standard deviations of the background noise level is plotted as a function of Doppler frequency using the orbital solution indicated in the figure. The spectra are sums of 15, 4, and 10 runs, respectively. Corrections to the ephemerides were used to update the orbit and are listed in Table 2. Each plot is shown at the same scale.

Echo power spectra were obtained on each day and are plotted in Fig. 1. The echoes were strong. The bandwidth was measured between the two frequencies where the echo power is 3-σ above the mean of the background noise. On June 28 and 29, the echoes have a similar bandwidth of 4 Hz. The bandwidth on July 4 increased to 5 Hz. This bandwidth change could be due to the shape of the object or to the change in the sub-radar latitude observed between June 28 and July 4 as the asteroid traversed 75 deg across the sky.

One notable feature in the CW spectra is the dip near 0 Hz seen on July 4. Using 10 runs and 85 FFTs to create the spectrum, which establishes that the noise distribution is Gaussian, this 10–15σ feature is statistically significant and is not receiver or "self" noise. This dip suggests the presence of a cavity. After completing the CW observations, there was a gap of ~20 min before the delay-Doppler imaging started. During this time, 2003 MS2 rotated approximately 17 deg, which may explain why this feature is not evident in the first delay-Doppler image in Fig. 2b. It is also possible that the dip is not visible in the images due to the frequency resolution. Another explanation for this feature is that it represents an area that is less reflective to the radar. Although radar albedo variations have not been seen before with observations of near-Earth asteroids, they have seen in radar observations of mainbelt asteroids (Shepard et al., 2010, 2015).

Fig. 2 shows delay-Doppler images from June 29 and July 4. The three images from June 29 show approximately 26 deg of rotation. The 19 m range resolution only coarsely resolves the asteroid; nevertheless, the images hint at an asymmetric shape. The observations on July 4 provide the longest sequence of images for this object. Each image in Fig. 2b is the weighted sum of 10 runs and the collage shows the asteroid rotating approximately 140 deg during the 2.7 h of radar imaging. This implies that the asteroid completes one full rotation in ~7 h, a result consistent with the period reported by Muinonen et al. (2007).

Unfortunately, there is insufficient data to perform detailed shape modeling with this data set because we did not obtain enough rotational coverage of the asteroid.

The July 4 images show that the shape of the echo is very angular with flat facets that give it a triangular appearance. The maximum and minimum bandwidths are 4.75 and 2.75 Hz and suggest an elongated object with an aspect ratio of $b/a = 0.58$. This is consistent with the ratio of <0.67 from Muinonen et al. (2007).

Panel 10 (middle row, at the far right) of Fig. 2 reveals a flat, horizontal feature. Such an echo is produced when the surface is nearly perpendicular to the radar line of site. The bandwidth of this feature is 3.00 Hz, and, if we adopt a rotation period of 7 h, it corresponds to a length of ~210 m/cos(δ).

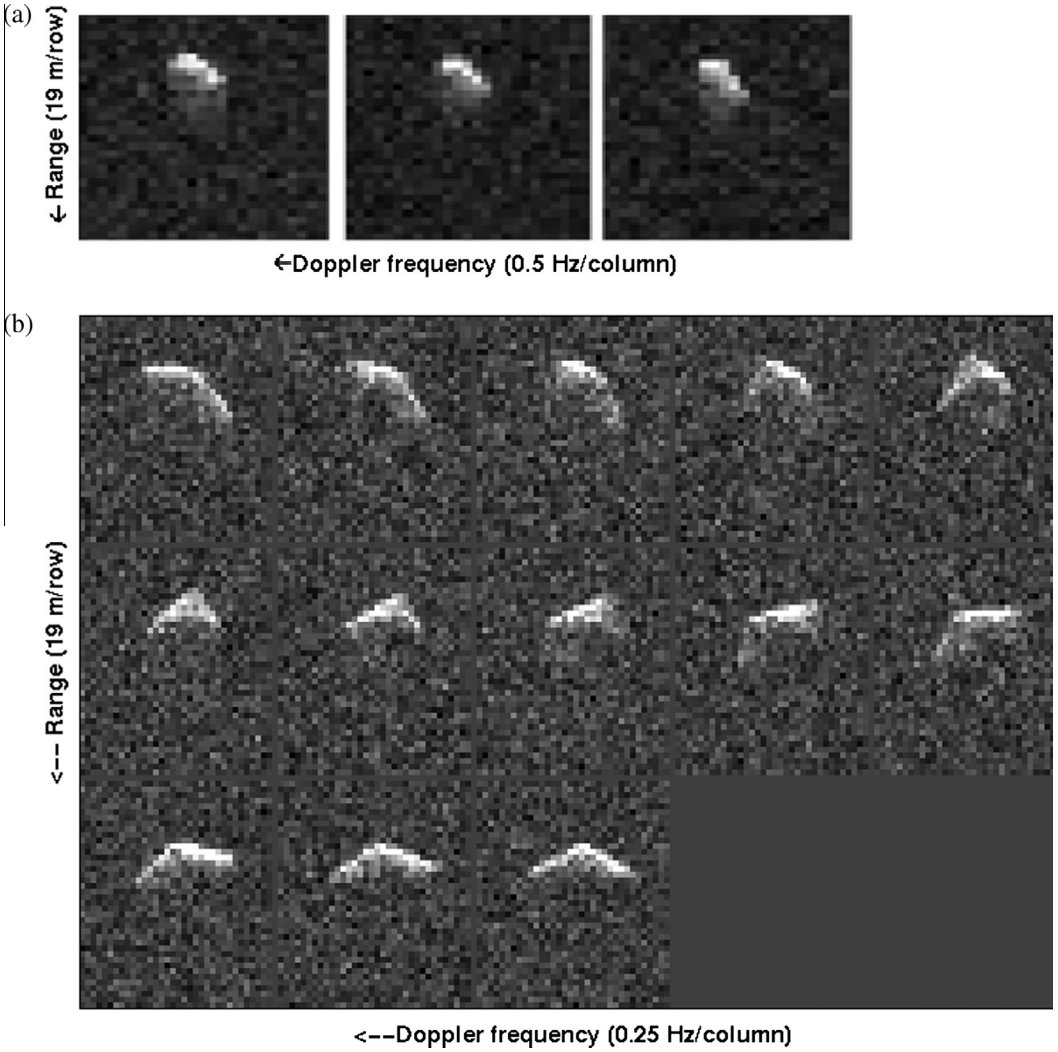

Fig. 2. Delay-Doppler radar images of 2003 MS2 acquired on (a) June 29 and (b) July 4, 2003. Range increases downward and Doppler frequency increases toward the left, so the rotation is clockwise. Time increases toward the right and downward. Each image is a sum of 10 runs.

We can constrain the dimensions of the asteroid from the visible extent of the echo by counting the number of consecutive pixels in time delay that are at least 3-σ above the noise level. For a spherical object, the visible extent corresponds to about one half of the diameter. The echo's visible extent varies between 110 m and 210 m, and if we assume that we see only one half of the true extent, then this corresponds to a maximum length of 420 m along its largest dimension. We can also estimate the pole-on dimensions by using the bandwidths, 7 h rotation period, and Eq. (1). The widest bandwidth of 4.75 Hz gives a maximum dimension of 333 m/cos δ, which is significantly smaller than the number obtained by doubling the visible extent. This apparent discrepancy is likely due to the asteroid's irregular shape. Similarly, a lower bound on the intermediate axis can be calculated from the minimum bandwidth, which gives a value of 190 m/cos δ.

In addition, we see no evidence that the observed subradar latitude was more than ±30 deg from the equator at the time of our observations. If the subradar latitudes were close to a pole-on orientation, then there would not be such a large difference in the visible extents and the bandwidths would be much more narrow.

In order to constrain the pole direction, we calculated the pole directions in 5 deg increments in ecliptic latitude β and longitude λ (Fig. 3) that result in subradar latitudes remaining within ±30 deg from the equator for the duration of our observing arc. The two dark gray areas in Fig. 3 show the candidate pole directions based on the radar data. As described in Ostro (1987), we can constrain the pole direction further by combining our solution with the pole constraints estimated from lightcurves by Muinonen et al. (2007), which appear in Fig. 3 as two light gray annuli. The intersection of the two regions further constrains the pole to two regions between (λ, β) = (20 ± 20 deg, 0 ± 40 deg) and (200 ± 20 deg, 0 ± 40 deg).

If we assume that 2003 MS2 is a biaxial ellipsoid with dimensions of 0.33 × 0.19 × 0.19 km, then the effective diameter (the diameter of a sphere with the same volume as that of the target) is 0.28 km. Using the relationship between the target's effective diameter, $D_{\rm eff}$ and absolute visual magnitude, H, (Bowell et al., 1989),

$$\log p_v = 6.259 - 2\log D_{\rm eff} - 0.4H \quad (2)$$

we obtain an optical albedo of 0.08. With a relatively low optical albedo, 2003 MS2 is unlikely to be a V- or E-class object, but this albedo is consistent with the dark spectral classes and perhaps with an M-class object.

Table 3
Disk-integrated radar properties.

Date	μ_c	σ_{OC} (km^2)	
2003 MS2			
2003 June 28	0.30 ± 0.03	0.017 ± 0.006	
2003 June 29	0.30 ± 0.02	0.021 ± 0.007	
2003 July 4	0.33 ± 0.02	0.014 ± 0.005	
Mean		0.017 ± 0.003	
μ_c for NEA spacecraft targets			
433 Eros	0.28 ± 0.06	G, A	Magri et al. (2001)
4179 Toutatis	0.29 ± 0.01	G	Ostro et al. (1999)
25143 Itokawa	0.27 ± 0.04	A	Ostro et al. (2004)
101955 Bennu	0.18 ± 0.01	G, A	Nolan et al. (2013)
NEA – Mean	0.34 ± 0.25		Benner et al. (2008)

Circular polarization ratios, μ_c, and radar OC cross-sectional values, σ_{OC}, of 2003 MS2 obtained on each day of the radar experiment. The circular polarization ratios of NEAs visited by spacecraft are listed for comparison. The observatories are identified as A for Arecibo and G for Goldstone.

Table 3 lists the daily radar cross sections. We assign a standard error value of 35% to account for uncertainties that are dominated by calibration and pointing errors. Over the coarse of the experiment, the average radar cross section of 2003 MS2 is 0.017 ± 0.003 km^2.

Finally, we estimate the opposite-sense radar albedo, $\hat{\sigma}_{OC}$, defined as:

$$\hat{\sigma}_{OC} = \sigma_{OC}/A = 4\sigma_{OC}/\pi D_{\rm eff}^2 \quad (3)$$

where A is the asteroid's projected area and $D_{\rm eff}$ is the effective diameter of a sphere with the same volume as the object. We obtain a radar albedo of 0.28. This is slightly above the average value of 0.20 ± 0.12 from a sample of 40 NEAs (see http://echo.jpl.nasa.gov/~lance/asteroid_radar_properties/nea.radaralbedo.html). It is consistent with albedo estimates for most of the spectral classes, but it is lower than would be expected for an object that is metallic.

The echo's circular polarization ratio, μ_c, is defined as the ratio of the echo power strengths in the two polarizations (SC/OC) and provides a gauge of the near-surface roughness at decimeter spatial scales. Table 3 lists the daily values of μ_c. 2003 MS2's average circular polarization ratio is 0.31 ± 0.02, indicating a near-surface roughness comparable to the mean NEA value (0.34) calculated from a sample of 214 objects (Benner et al., 2008). Listed for comparison are ratios for NEAs visited by spacecraft and 101955 Bennu, the future target of the OSIRIS-REx mission. 2003 MS2's

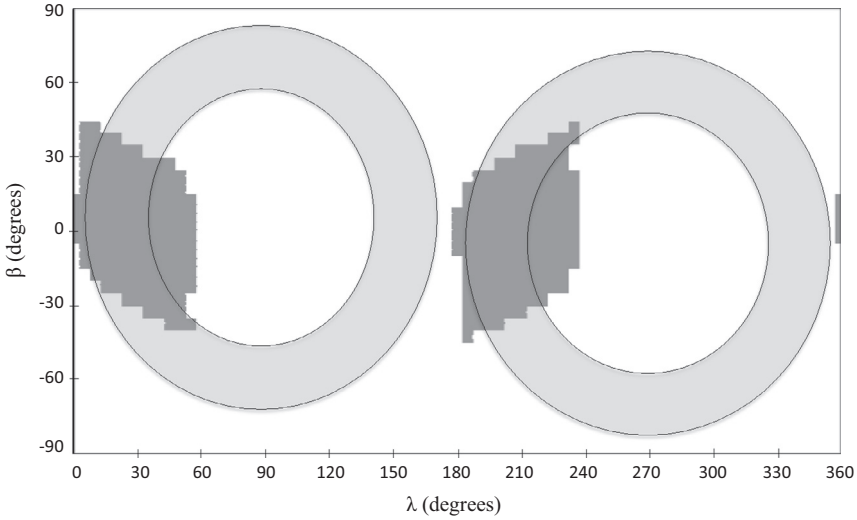

Fig. 3. Constraints on the pole direction. Dark gray areas show constraints on the pole direction from the radar data. The two annuli show constraints estimated from lightcurves by Muinonen et al. (2007). The intersections between the two regions provide the best constraints.

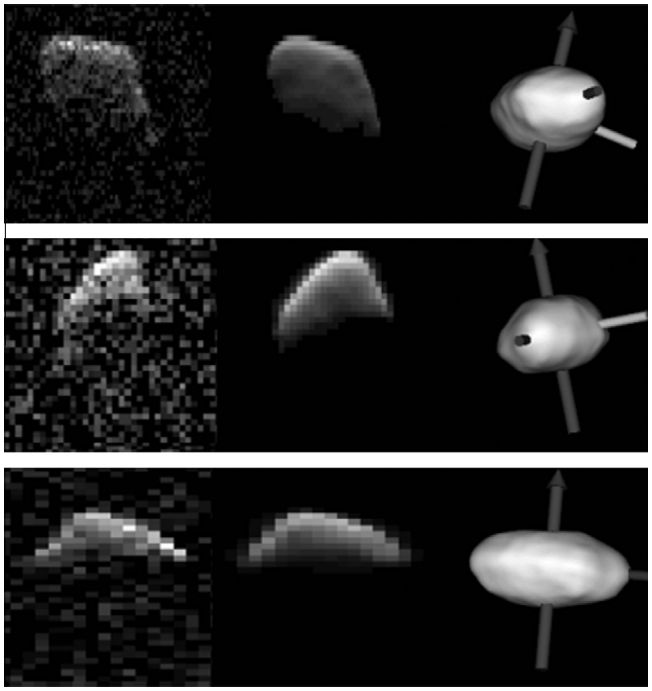

Fig. 4. Selected images of the preferred model of (4660) Nereus from Brozovic et al. (2009). The delay-Doppler images are in the left column, the images synthesized from the shape model are in the middle column, and the model's plane of sky views are on the right. The arrows indicate the positive ends of the long and intermediate axes and illustrate the orientation of the spin vector.

circular polarization ratio is similar to that of 25143 Itokawa and 4179 Toutatis but is larger than the one obtained for Bennu by nearly a factor of two, suggesting a more complex near-surface.

4. Discussion

Facets, linear, and angular features have been seen in radar images of NEAs 6489 Golevka (Hudson et al., 2000), 25143 Itokawa (Ostro et al., 2005), 54509 YORP (Taylor et al., 2007), 29075 1950 DA (Busch et al., 2007), and 4660 Nereus (Brozovic et al., 2009), establishing that such features are not rare. Several images of 2003 MS2 show an angular leading edge. At higher resolutions, some of these features on other NEAs have appeared less angular, so it is possible that this is also true with 2003 MS2. For comparison, Nereus appears angular in some radar images and a 3D shape model is available (Brozovic et al., 2009). The model of Nereus lacks sharp edges, although one end is more angular than the other (Fig. 4). The angular features seen in the 2003 MS2 data appear similar to those on Nereus and may result from angular or shape attributes as well.

2003 MS2 is one of the most angular sub-kilometer NEAs imaged by radar. How did it form? It is plausible that 2003 MS2 is a fragment that was split off from a larger body due to a collision. If it is a shard, then 2003 MS2's angular shape seems inconsistent with a rubble pile internal structure. Hudson et al. (2000) speculated that the angularity of Golevka suggests that it is not a rubble pile and is instead an impact-generated fragment formed as a result of collision.

Could 2003 MS2 be a rubble pile? With such a limited data set, we cannot rule this out. Early rubble pile simulations used spherical or ellipsoidal elements (Leinhardt et al., 2000; Michel and Richardson, 2013 and references therein) that produced rounded shapes. Korycansky and Asphaug (2006) modeled low speed impacts between polyhedral rubble piles. We are unaware of any simulations that produce the angularity of 2003 MS2. Perhaps the simulations lack sufficient sophistication to produce objects this angular. To more meaningfully investigate the surface and angular features of 2003 MS2, as well as its origins, future radar and optical observations providing thorough rotational coverage are essential so that a shape model can be estimated.

During the discovery apparition, the time-span over which it was possible to reliably predict close Earth encounters within ±10 days or ±0.1 au (3σ uncertainties) using only optical astrometry was 206 years from 1934 to 2140. After the radar astrometry was included in the orbit solution, this interval increased 369 years (179%) from 1664 to 2239. 2003 MS2 was also observed optically in 2005 and its interval of reliable Earth-encounter predictability

Table 4
Past and future close approaches of 2003 MS2.

Date (CT)	CA Dist (au)	MinDist (au)	MaxDist (au)	Vrel (km/s)	TCA3Sg (min)
1580 June 16.68692	0.033390	0.030584	0.045698	11.202	1836.4
1597 June 27.87543	0.030029	0.030024	0.030285	11.050	299.64
1614 June 30.11324	0.043118	0.038809	0.047914	10.780	587.32
1664 June 27.56993	0.029166	0.029144	0.029190	11.072	26.71
1731 June 29.51979	0.028115	0.028112	0.028119	11.064	17.58
1798 June 29.55038	0.027064	0.027063	0.027064	11.030	2.09
1848 June 27.66613	0.047798	0.047539	0.048058	11.490	25.74
1865 June 29.71733	0.027818	0.027809	0.027827	11.139	2.25
1882 June 28.87393	0.038816	0.038731	0.038901	11.351	9.37
1934 July 01.67079	0.025014	0.025014	0.025015	11.043	2.60
1986 July 03.06938	0.033433	0.033416	0.033451	10.841	2.23
2003 July 02.48554	**0.025303**	**0.025303**	**0.025303**	**10.964**	**0.01**
2070 June 30.98021	0.027927	0.027923	0.027931	11.200	0.54
2139 July 03.67407	0.023374	0.023367	0.023381	10.962	1.74
2156 July 04.52582	0.040962	0.040754	0.041171	10.740	20.24
2206 July 04.93151	0.025620	0.025454	0.025788	10.897	23.84
2239 July 05.14590	0.024510	0.023700	0.025394	10.907	126.88
2288 July 06.03074	0.045576	0.035948	0.055882	10.696	902.46
2304 July 04.75430	0.019698	0.019698	0.021153	11.028	589.88
2320 July 03.00548	0.038440	0.019626	0.145392	11.369	8850.4

Past and future close approaches to Earth, at distances less than 0.05 au, from 1564 through the year 2320. The nominal close-approach distance, CA Dist, is the geometric close-approach distance. MinDist and MaxDist are the three-sigma minimum and maximum closest-approach distance possible. The relative velocity, Vrel, of the object and Earth are provided. TCA3Sg is the three-sigma uncertainty in the close-approach time. There are an additional 36 approaches with the close approach distance in the range of 0.05 au < Δ < 0.10 au during this period. Results are from a numerical integration that considers point-mass gravity perturbations of the planets, Moon, and the 16 most massive asteroids.
The radar observations discussed in this paper were taken in June and July 2003 near the date, highlighted in bold, when asteroid 2003 MS2 was at its closest approach.

currently spans 756 years from 1564 to 2320. Within this time period, twenty close approaches come within 0.05 au of the Earth (Table 4). There are an additional 36 approaches in the range of 0.05 au < Δ < 0.10 au. 2003 MS2 makes close approaches to the Earth at intervals of approximately 17 years. The closest nominal approach over the entire interval of reliable orbit estimations will be at 0.02 au on July 4, 2304. This deep encounter will cause the orbital uncertainties to grow rapidly afterward.

5. Future observation opportunities

The next flyby close enough for radar observations will occur in July 2020 at 0.078 au. The signal-to-noise ratio should exceed 300 per day at Arecibo operating under standard conditions (i.e., transmitter power of 900 kW, and system temperature of 23 K). This should allow observations at resolutions as high as 15 m/pixel. During the weeks prior to this, the object will be at an approximate visual magnitude of 19.5 and solar elongations of 70 deg when optical observations will be possible, but challenging. Until this time, the asteroid is faint for optical telescopes, never reaching visual magnitudes brighter than 21.6. The next Earth flyby at a distance comparable to the approach in 2003 will be in June 2070 at a distance of 0.028 au.

Acknowledgments

We thank the technical and support staff of Goldstone for their assistance with the observations. Comments by reviewers Patrick Taylor and Chris Magri significantly improved this paper. This research was conducted at the Jet Propulsion Laboratory, California Institute of Technology, under contract with the National Aeronautics and Space Administration (NASA). The material presented represents work supported by NASA under the Science Mission Directorate Research and Analysis Programs.

References

Benner, L.A.M. et al., 2008. Near-Earth asteroid surface roughness depends on compositional class. Icarus 198, 294–304.
Bowell, E.B. et al., 1989. Application of photometric models to asteroids. In: Binzel, R.P., Gehrels, T., Mathews, M.S. (Eds.), Asteroids II. Univ. of Arizona Press, Tuscon, pp. 524–556.
Brozovic, M. et al., 2009. Radar observations and a physical model of Asteroid 4660 Nereus, a prime space mission target. Icarus 201, 153–166.
Busch, M.W. et al., 2007. Physical modeling of near-Earth Asteroid (29075) 1950 DA. Icarus 190, 608–621.
Hudson, R.S. et al., 2000. Radar observations and physical model of Asteroid 6489 Golevka. Icarus 148, 37–51.
Korycansky, D.G., Asphaug, E., 2006. Low-speed impacts between rubble piles modeled as collections of polyhedra. Icarus 181, 605–617.
Leinhardt, Z.M., Richardson, D.C., Quinn, T., 2000. Direct N-body simulations of rubble pile collisions. Icarus 146, 133–151.
Magri, C. et al., 2001. Radar constraints on asteroid regolith properties using 433 Eros as ground truth. Meteorit. Planet. Sci. 36, 1697–1709.
Michel, P., Richardson, D.C., 2013. Collision and gravitational reaccumulations: Possible formation mechanism of the asteroid Itokawa. Astron. Astrophys. 554, 1–4.
Muinonen, K. et al., 2007. Spins, shapes, and orbits for near-Earth objects by Nordic NEON. In: Milani, A., Valsecchi, G.B., Vokrouhlický, D. (Eds.), Near Earth Objects, our Celestial Neighbors: Opportunity and Risk. Cambridge University Press, Cambridge, pp. 309–320.
Nolan, M.C. et al., 2013. Shape model and surface properties of the OSIRIS-REx target Asteroid (101955) Bennu from radar and lightcurve observations. Icarus 226, 629–640.
Ostro, S.J., 1987. Physical properties of asteroids from radar observations. In: Fulchignoni, M., Kresák, L. (Eds.), The Evolution of the Small Bodies of the Solar System, Proceedings of the International School of Physics "Enrico Fermi". North-Holland, Amsterdam, pp. 131–146.
Ostro, S.J., 1993. Planetary radar astronomy. Rev. Mod. Phys. 65, 1235–1279.
Ostro, S.J. et al., 1999. Asteroid 4179 Toutatis: 1996 radar observations. Icarus 137, 122–139.
Ostro, S.J. et al., 2004. Radar observations of Asteroid 25143 Itokawa (1998 SF36). Meteorit. Planet. Sci. 39, 407–424.
Ostro, S.J. et al., 2005. Radar observations of Itokawa in 2004 and improved shape estimation. Meteorit. Planet. Sci. 40, 1563–1574.
Shepard, M.K. et al., 2010. A radar survey of M- and X-class asteroids II. Summary and synthesis. Icarus 208, 221–231.
Shepard, M.K. et al., 2015. A radar survey of M- and X-class asteroids. III Insights into their composition, hydration state and structure. Icarus 245, 38–55.
Taylor, P.A. et al., 2007. Spin rate of Asteroid (54509) 2000 PH5 increasing due to the YORP effect. Science 316, 274–277.